PFNN: A Penalty-Free Neural Network Method for Solving a Class of Second-Order Boundary-Value Problems on Complex Geometries

Hailong Sheng[a,c], Chao Yang[b,*]

[a] *Institute of Software, Chinese Academy of Sciences, Beijing 100190, China*
[b] *School of Mathematical Sciences, Peking University, Beijing 100871, China*
[c] *University of Chinese Academy of Sciences, Beijing 100190, China*

arXiv:2004.06490v1 [math.NA] 14 Apr 2020

Abstract

We present PFNN, a penalty-free neural network method, to efficiently solve a class of second-order boundary-value problems on complex geometries. To reduce the smoothness requirement, the original problem is reformulated to a weak form so that the evaluations of high-order derivatives are avoided. Two neural networks, rather than just one, are employed to construct the approximate solution, with one network satisfying the essential boundary conditions and the other handling the rest part of the domain. In this way, an unconstrained optimization problem, instead of a constrained one, is solved without adding any penalty terms. The entanglement of the two networks is eliminated with the help of a length factor function that is scale invariant and can adapt with complex geometries. We prove the convergence of the PFNN method and conduct numerical experiments on a series of linear and nonlinear second-order boundary-value problems to demonstrate that PFNN is superior to several existing approaches in terms of accuracy, flexibility and robustness.

Keywords: Deep neural network, Penalty-free method, Boundary-value problem, Partial differential equation, Complex geometry

1. Introduction

During the past decade, neural network is gaining increasingly more attention from the big data and artificial intelligence community [1, 2, 3], and playing a central role in a broad range of applications related to, e.g., image processing [4], computer vision [5] and natural language processing [6]. However, in scientific and engineering computing, the studying of neural networks is still at an early stage. Recently, thanks to the introduction of deep neural networks, successes have been achieved in a series of challenging tasks, including turbulence modeling [7, 8], molecular dynamics simulations [9, 10], and solutions of stochastic and high-dimensional partial differential equations [11, 12, 13, 14]. In addition to that, a great deal of efforts are also made to build the connections between neural networks

*Corresponding author.
Email addresses: hailong2019@iscas.ac.cn (Hailong Sheng), chao_yang@pku.edu.cn (Chao Yang)

and traditional numerical methods such as finite element [15], wavelet [16], multigrid [17], hierarchical matrices [18, 19] and domain decomposition [20] methods. However, it is still far from clear whether neural networks can solve ordinary/partial differential equations and truly exhibit advantages as compared to classical discretization schemes in accuracy, flexibility and robustness.

An early attempt on utilizing neural network methods to solve differential equations can be traced back to three decades ago [21], in which a Hopfield neural network was employed to represent the discretized solution. Shortly afterwards, methodologies to construct closed form numerical solutions with neural networks were proposed [22, 23]. Since then, more and more efforts were made in solving differential equations with various types of neural networks, such as feedforward neural network [24, 25, 26, 27], radial basis network [28, 29], finite element network [30], cellular network [31], and wavelet network [32]. These early studies have in certain ways illustrated the feasibility and effectiveness of neural network based methods, but are limited to handling model problems with regular geometry in low space dimensions. Moreover, the networks utilized in these works are relatively shallow, usually containing only one hidden layer, whereas the potential merits of the deep neural networks are not fully revealed.

Nowadays, with the advent of the deep learning technique [33, 34, 35], neural networks with substantially more hidden layers have become valuable assets. Various challenging problems modeled by complex differential equations have been taken into considerations and successfully handled by neural network based methods [36, 37, 38, 39, 40, 41, 42, 43, 44, 45]. These remarkable progresses have demonstrated the advantages of deep neural networks in terms of the strong representation capability. However, the effectiveness of the neural network based methods are still hindered by several factors. Specifically, the accuracy of the neural network based approximation as well as the efficiency of the training task usually have a strong dependency on the properties of the problems, such as the nonlinearity of the equation, the irregularity of the solution, the shape of the boundary, the dimension of the domain, among other factors. It is therefore of paramount importance to improve the robustness and flexibility of the neural network based approaches. For instance, several methods [36, 37, 38, 20] have been recently proposed to transform the original problem into a corresponding weak form, thus lowering the smoothness requirement and possibly reducing the cost of the training process. Unfortunately, in these works extra penalty terms due to the boundary constraints are included in the loss function, which could eventually have a negative effect on the training process and the achievable accuracy. On the other hand, a number of efforts [24, 25, 26, 27] were made to explicitly manufacture the numerical solution so that the boundary conditions can be automatically satisfied. However, the construction processes are usually limited to problems with simple geometries, not flexible enough to generalize to arbitrary domains with arbitrary boundary conditions.

In this work, we propose PFNN, a penalty-free neural network method, for solving a class of second-order boundary-value problems on complex geometries. In order to reduce the smoothness requirement, we reformulate the original problem to a weak form so that the approximation of high-order derivatives of the solution is avoided. In order to adapt with various boundary constrains without adding any penalty terms, we employ two networks,

rather than just one, to construct the approximate solution, with one network satisfying the essential boundary conditions and the other handling the rest part of the domain. And in order to disentangle the two networks, a length factor function is introduced to eliminate the interference between them so as to make the method applicable to arbitrary geometries. We prove that the proposed method converges to the true solution of the boundary-value problem as the number of hidden units of the networks increases, and show by numerical experiments that PFNN can be applied to a series of linear and nonlinear second-order boundary value problems. Compared to existing approaches, the proposed method is able to produce more accurate solutions with fewer unknowns and less training costs.

The remainder of the paper is organized as follows. In Section 2, the basic framework of the PFNN method is presented. Following that we provide some theoretical analysis results on the accuracy of the PFNN method in Section 3. Some further comparisons between the present work and several recently proposed methods can be found in Section 4. We report numerical results on various second-order boundary value problems in Section 5. The paper is concluded in Section 6.

2. The PFNN method

Consider the following boundary-value problem:

$$\begin{cases} -\nabla\cdot\Big(\rho(|\nabla u|)\nabla u\Big)+h(u)=0, & \text{in } \Omega\subset\mathbb{R}^d,\\ u=\varphi, & \text{on } \Gamma_D,\\ \Big(\rho(|\nabla u|)\nabla u\Big)\cdot\boldsymbol{n}=\psi, & \text{on } \Gamma_N, \end{cases} \tag{1}$$

where $\boldsymbol{n}$ is the outward unit normal, $\Gamma_D\cup\Gamma_N=\partial\Omega$ and $\Gamma_D\cap\Gamma_N=\varnothing$.

It is well understood that under certain conditions (1) can be seen as the Euler-Lagrange equation of the energy functional

$$I[w]:=\int_\Omega\left(P(w)+H(w)\right)d\boldsymbol{x}-\int_{\Gamma_N}\psi w d\boldsymbol{x}, \tag{2}$$

where

$$P(w):=\int_0^{|\nabla w|}\rho(s)sds\quad\text{and}\quad H(w):=\int_0^w h(s)ds. \tag{3}$$

Introducing a hypothesis space $\mathcal{H}$ constructed with neural networks, the approximate solution u^* is obtained by solving the following minimization problem:

$$u^*=\arg\min_{w\in\mathcal{H}}\Psi[w], \tag{4}$$

where

$$\Psi[w]:=\frac{|\Omega|}{\#S(\Omega)}\sum_{\boldsymbol{x}^i\in S(\Omega)}\Big(P(w(\boldsymbol{x}^i))+H(w(\boldsymbol{x}^i))\Big)-\frac{|\Gamma_N|}{\#S(\Gamma_N)}\sum_{\boldsymbol{x}^i\in S(\Gamma_N)}\psi(\boldsymbol{x}^i)w(\boldsymbol{x}^i) \tag{5}$$

is the loss function representing the discrete counterpart of $I[w]$, $S(\square)$ denotes a set of sampling points on $\square$, and $\#S(\square)$ is the size of $S(\square)$.

In this work, the hypothesis space $\mathcal{H}$ is not an arbitrary space formed by neural networks. Instead, it is designed to encapsulate the essential boundary conditions. To construct the approximate solution $w_{\boldsymbol{\theta}} \in \mathcal{H}$, we employ two neural networks, $g_{\boldsymbol{\theta_1}}$ and $f_{\boldsymbol{\theta_2}}$, instead of one, such that

$$w_{\boldsymbol{\theta}}(\boldsymbol{x}) = g_{\boldsymbol{\theta_1}}(\boldsymbol{x}) + \ell(\boldsymbol{x}) f_{\boldsymbol{\theta_2}}(\boldsymbol{x}), \tag{6}$$

where $\boldsymbol{\theta} = \{\boldsymbol{\theta_1}, \boldsymbol{\theta_2}\}$ is the collection of the weights and biases of the two networks, and ℓ is a length factor function for measuring the distance to Γ_D, which satisfies

$$\begin{cases} \ell(\boldsymbol{x}) = 0, & \boldsymbol{x} \in \Gamma_D, \\ \ell(\boldsymbol{x}) > 0, & \text{otherwise}. \end{cases} \tag{7}$$

With the help of the length factor function, the neural networks $g_{\boldsymbol{\theta_1}}$ and $f_{\boldsymbol{\theta_2}}$ are utilized to approximate the true solution u on the essential boundary Γ_D and the rest of the domain, respectively. The training of $g_{\boldsymbol{\theta_1}}$ and $f_{\boldsymbol{\theta_2}}$ are conducted separately, where $g_{\boldsymbol{\theta_1}}$ is trained on the essential boundary to minimize the following energy functional

$$\Phi[g_{\boldsymbol{\theta_1}}] := \sum_{\boldsymbol{x}^i \in S(\Gamma_D)} \left(\varphi(\boldsymbol{x}^i) - g_{\boldsymbol{\theta_1}}(\boldsymbol{x}^i)\right)^2, \tag{8}$$

and $f_{\boldsymbol{\theta_2}}$ is trained to approximate u on the rest of the domain by minimizing the loss function (5) By this means, $f_{\boldsymbol{\theta_2}}$ would not produce any influence on Γ_D, and the interference between the two networks are eliminated.

To construct the length factor function ℓ, the boundary of the domain is divided into n segments: γ_k $(k = 1, 2, \cdots, n,\ n \geq 4)$, with each segment either belonging to Γ_D or to Γ_N. For any boundary segment $\gamma_k \subset \Gamma_D$, select another segment γ_{k_o} $(k_o \in \{1, 2, \cdots, n\}$, $k_o \neq k)$, which is not the neighbor of γ_k, as its companion. After that, for each $\gamma_k \subset \Gamma_D$, we construct a spline function l_k that satisfies

$$\begin{cases} l_k(\boldsymbol{x}) = 0, & \boldsymbol{x} \in \gamma_k, \\ l_k(\boldsymbol{x}) = 1, & \boldsymbol{x} \in \gamma_{k_o}, \\ 0 < l_k(\boldsymbol{x}) < 1, & \text{otherwise}. \end{cases} \tag{9}$$

Then ℓ is defined as:

$$\ell(\boldsymbol{x}) = \frac{\widetilde{\ell}(\boldsymbol{x})}{\max\limits_{\boldsymbol{x} \in \Omega} \widetilde{\ell}(\boldsymbol{x})}, \quad \text{where} \quad \widetilde{\ell}(\boldsymbol{x}) = \prod_{k \in \{k | \gamma_k \subset \Gamma_D\}} 1 - (1 - l_k(\boldsymbol{x}))^{\mu}. \tag{10}$$

Here a hyper-parameter $\mu \geq 1$ is introduced to adjust the shape of ℓ. A suggested value is $\mu = n_{\gamma_D}$, i.e., the number of the boundary segments on Γ_D, since in this way the average value of ℓ is kept in a proper range and would not decrease dramatically with the increase of n_{γ_D}.

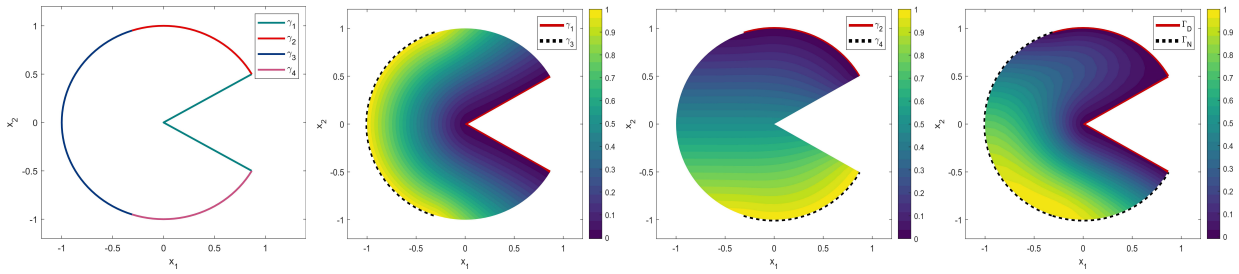

(a) Boundary (b) l_1 (c) l_2 (d) ℓ ($\mu = 2$)

Figure 1: An illustration on the construction of the length factor function ℓ for the case of a slotted disk.

For the purpose of flexibility, we employ the radial basis interpolation [46], among other choices, to construct l_k. Taking m_k distinct points $\widehat{\boldsymbol{x}}^{k,1}, \widehat{\boldsymbol{x}}^{k,2}, \cdots, \widehat{\boldsymbol{x}}^{k,m_k} \in \gamma_k \cup \gamma_{k_o}$ as the interpolation nodes, l_k is defined as:

$$l_k(\boldsymbol{x}) = \sum_{i=1}^{m_k} a_i \phi(\boldsymbol{x}; \widehat{\boldsymbol{x}}^{k,i}) + \boldsymbol{b} \cdot \boldsymbol{x} + c, \tag{11}$$

where

$$\phi(\boldsymbol{x}; \widehat{\boldsymbol{x}}) = \left(e^2 + \|\boldsymbol{x} - \widehat{\boldsymbol{x}}\|^2\right)^{-1/2} \tag{12}$$

is an inverse multiquadric radial basis function. Here the parameter e is used to adjust the shape of ϕ, To maintain scale invariance, which is important for solving differential equations, we set $e = 1.25R/\sqrt{m_k}$, where R is the radius of the minimal circle that encloses all the interpolation nodes. Similar configurations of e have been suggested in several previous studies such as [47, 48]. The coefficients $a_i, \boldsymbol{b}$ and c are determined by solving a small linear system defined by the following constraints:

$$\sum_{i=1}^{m_k} a_i \widehat{\boldsymbol{x}}^{k,i} = \boldsymbol{0}, \quad \sum_{i=1}^{m_k} a_i = 0, \quad l_k(\widehat{\boldsymbol{x}}^{k,i}) = \begin{cases} 0, & \widehat{\boldsymbol{x}}^{k,i} \in \gamma_k, \\ 1, & \widehat{\boldsymbol{x}}^{k,i} \in \gamma_{k_o}, \end{cases} \quad \forall i \in \{1, \cdots, m_k\}. \tag{13}$$

In particular, if γ_k and γ_{k_o} are two parallel hyper-planes, l_k is reduced to a linear polynomial, which can be derived analytically without interpolation.

To further illustrate how the length factor function ℓ is constructed, consider an example that Ω is a slotted disk as shown in Figure 1. Suppose the whole boundary $\partial\Omega = \Gamma_D \cup \Gamma_N$ is divided into four segments such that $\Gamma_D = \gamma_1 \cup \gamma_2$ and $\Gamma_N = \gamma_3 \cup \gamma_4$, where γ_3 and γ_4 are the opposite sides of γ_1 and γ_2, respectively. One can build l_1 and l_2 according to (11)-(13) and then construct ℓ with (10).

3. Theoretical analysis of PFNN method

In this section, we provide a theoretical proof to verify that under certain conditions the approximate solution obtained by the PFNN method is able to converge to the true solution

of the boundary-value problem (1) as the number of hidden units in the neural networks $g_{\boldsymbol{\theta_1}}$ and $f_{\boldsymbol{\theta_2}}$ increases.

We suppose that the true solution of (1) belongs to the function space

$$\mathcal{W}_D^{1,p}(\Omega) := \{w \in \mathcal{W}^{1,p}(\Omega) | w = \varphi \text{ on } \Gamma_D\}, \tag{14}$$

where $\mathcal{W}^{1,p}(\Omega) := \{w | \|w\|_{1,p,\Omega} < \infty\}$, $\|w\|_{1,p,\Omega} := \left(\int_\Omega (|w|^p + |\nabla w|^p)\, d\boldsymbol{x}\right)^{1/p}$. Further, it is assumed that the function $\rho(\cdot)\cdot$ in (1) satisfies the following conditions:

(i) $\rho(\cdot)\cdot$ is strictly increasing on $\mathbb{R}^+$ and $\rho(s)s|_{s=0} = 0$.

(ii) there exist constants $p > 1$, $\lambda_1 > 0$ and $\lambda_2 \geq 0$, such that for all $s \in \mathbb{R}^+$, $\rho(s)s \leq \lambda_1 s^{p-1} - \lambda_2$.

(iii) $\rho(\cdot)\cdot$ is Hölder continuous. If $1 < p \leq 2$, there exists a constant $C_1 > 0$, such that

$$|\rho(s_1)s_1 - \rho(s_2)s_2| \leq C_1 |s_1 - s_2|^{p-1},\ \forall s_1, s_2 \in \mathbb{R}^+; \tag{15}$$

otherwise, there exist constants $C_1 > 0$, $K_1 \geq 0$ and $K_2 > 0$, such that

$$|\rho(s_1)s_1 - \rho(s_2)s_2| \leq C_1 |s_1 - s_2|(K_1 + K_2(s_1 + s_2)^{p-2}),\ \forall s_1, s_2 \in \mathbb{R}^+. \tag{16}$$

(iv) If $1 < p \leq 2$, there exist constants $C_2 > 0$, $K_1 \geq 0$ and $K_2 > 0$, such that

$$(\rho(s_1)s_1 - \rho(s_2)s_2)(K_1 + K_2(s_1 + s_2)^{2-p}) \geq C_2(s_1 - s_2),\ \forall s_1 \geq s_2 \geq 0; \tag{17}$$

otherwise, there exists a constant $C_2 > 0$, such that

$$\rho(s_1)s_1 - \rho(s_2)s_2 \geq C_2(s_1^{p-1} - s_2^{p-1}),\ \forall s_1 \geq s_2 \geq 0. \tag{18}$$

Also, we assume that the function $h(\cdot)$ is monotonic increasing on $\mathbb{R}$ and satisfies conditions similar to (15)-(16).

We list two useful lemmas here for subsequent usage, among which the second one is the famous universal approximation property of the neural networks.

Lemma 1 (Chow, 1989, [49]) Suppose that the energy functional I is in the form of (2), $u = \arg \min_{w \in \mathcal{W}_D^{1,p}(\Omega)} I[w]$, $u^* = \arg \min_{w \in \mathcal{H}} I[w]$. Then there exists a constant $C > 0$, such that

$$\begin{cases} |u - u^*|_{1,p,\Omega}^2 \leq C\|u - u^*\|_{1,p,\Omega}^{p-1} \inf_{w \in \mathcal{H}} \|u - w\|_{1,p,\Omega}, & 1 < p \leq 2, \\ |u - u^*|_{1,p,\Omega}^p \leq C\|u - u^*\|_{1,p,\Omega} \inf_{w \in \mathcal{H}} \|u - w\|_{1,p,\Omega}, & p > 2. \end{cases} \tag{19}$$

Especially, if $\mathcal{H} \subset \mathcal{W}_D^{1,p}(\Omega)$, then $u - u^* \in W_0^{1,p}(\Omega) := \{w | w \in \mathcal{W}^{1,p}(\Omega) \text{ and } w = 0,\ \text{on } \Gamma_D\}$. In this case, there exists a constant C_3 such that $\|u - u^*\|_{1,p,\Omega} \leq C_3 |u - u^*|_{1,p,\Omega}$. Then we have

$$\|u - u^*\|_{1,p,\Omega} \leq \widetilde{C} \inf_{w \in \mathcal{H}} \|u - w\|_{1,p,\Omega}^s, \tag{20}$$

where $\widetilde{C} = C_3 C$, $s = 1/(3-p)$ if $1 < p \leq 2$ and $s = 1/(p-1)$ if $p > 2$.

Lemma 2 (K. Hornik, 1991 [50]) Let

$$\mathcal{F}^n := \{f_{\boldsymbol{\theta}} |\ f(\boldsymbol{x}; \boldsymbol{\theta}) = \sum_{j=1}^{i} a_j \sigma(\boldsymbol{w}_j \cdot \boldsymbol{x} + b_j),\ i \leq n\} \tag{21}$$

be the space consisting of all neural networks with single hidden layer of no more than n hidden units, where $\boldsymbol{\theta} = \{\boldsymbol{w}_j, a_j, b_j, j = 1, 2, \cdots, i\}$, $\boldsymbol{w}_j$ is the input weight, a_j is the output weight and b_j is the bias. If $\sigma \in \mathcal{W}^{m,p}(\Omega)$ is nonconstant and all its derivatives up to order m are bounded, then for all $f \in \mathcal{W}^{m,p}(\Omega)$ and $\varepsilon > 0$, there exists an integer $n > 0$ and a function $f_{\widehat{\boldsymbol{\theta}}} \in \mathcal{F}^n$, such that

$$\|f - f_{\widehat{\boldsymbol{\theta}}}\|_{m,p,\Omega} < \varepsilon. \tag{22}$$

The main convergence theorem of the PFNN method is given below.

Theorem 1 Suppose that the energy functional I is in the form of (2), $u = \arg \min_{w \in \mathcal{W}_D^{1,p}(\Omega)} I[w]$, $g^{n_1} = \arg \min_{g_{\boldsymbol{\theta_1}} \in \mathcal{F}^{n_1}} \int_{\Gamma_D} (\varphi - g_{\boldsymbol{\theta_1}})^2 dx$, $u^{n_1,n_2} = \arg \min_{w_{\boldsymbol{\theta}} \in \mathcal{H}^{n_1,n_2}} I[w_{\boldsymbol{\theta}}]$, where $\mathcal{H}^{n_1,n_2} := \{w_{\boldsymbol{\theta}} | w_{\boldsymbol{\theta}} = g^{n_1} + \ell f_{\boldsymbol{\theta_2}},\ f_{\boldsymbol{\theta_2}} \in \mathcal{F}^{n_2}\}$, then

$$\|u - u^{n_1,n_2}\|_{1,p,\Omega} \to 0 \quad \text{as} \quad n_1 \to \infty \text{ and } n_2 \to \infty. \tag{23}$$

Proof For the sake of brevity, we drop the subscripts in $w_{\boldsymbol{\theta}}$, $g_{\boldsymbol{\theta_1}}$ and $f_{\boldsymbol{\theta_2}}$ and utilize w, g and f to represent them, respectively. We only need to consider the case of $1 < p \leq 2$ since the proof for the case of $p > 2$ is analogous. Combining the Friedrichs' inequality with Lemma 1, we have

$$\begin{aligned} \|u - u^{n_1,n_2}\|_{1,p,\Omega} &\leq C_4 \left(|u - u^{n_1,n_2}|_{1,p,\Omega} + \|u - u^{n_1,n_2}\|_{0,2,\Gamma_D}\right) \\ &\leq C_5 \left(\|u - u^{n_1,n_2}\|_{1,p,\Omega}^{(p-1)/2} \inf_{w \in \mathcal{H}^{n_1,n_2}} \|u - w\|_{1,p,\Omega}^{1/2} + \|u - u^{n_1,n_2}\|_{0,2,\Gamma_D} \right), \end{aligned} \tag{24}$$

where C_4, C_5 are constants.

First, we prove that $\|u - u^{n_1,n_2}\|_{0,2,\Gamma_D} \to 0$ as $n_1 \to \infty$, for arbitrary $n_2 \in \mathbb{N}^+$. According to Lemma 2, for all $\varepsilon > 0$, there exists an integer $n_1^* > 0$ and a function $\widehat{g} \in \mathcal{F}^{n_1^*}$ satisfying $\|\varphi - \widehat{g}\|_{0,2,\Gamma_D} < \varepsilon$. Due to $g^{n_1} = \arg \min_{g \in \mathcal{F}^{n_1}} \int_{\Gamma_D} (\varphi - g)^2 dx = \arg \min_{g \in \mathcal{F}^{n_1}} \|\varphi - g\|_{0,2,\Gamma_D}$, the following relationship hold:

$$\|u - u^{n_1,n_2}\|_{0,2,\Gamma_D} = \|\varphi - g^{n_1}\|_{0,2,\Gamma_D} \leq \|\varphi - \widehat{g}\|_{0,2,\Gamma_D} < \varepsilon, \quad \forall\ n_1 \geq n_1^*. \tag{25}$$

We then prove that $\inf_{w \in \mathcal{H}^{n_1,n_2}} \|u - w\|_{1,p,\Omega}^{1/2} \to 0$ as $n_2 \to \infty$, for arbitrary $n_1 \in \mathbb{N}^+$. Since u, g^{n_1}, $\ell \in \mathcal{W}^{1,p}(\Omega)$ and $\ell > 0$, in Ω, we have $\dfrac{u - g^{n_1}}{\ell} \in \mathcal{W}^{1,p}(\Omega)$. According to Lemma

2, for all $\varepsilon > 0$ and $n_1 > 0$, there exists an integer $n_2^* > 0$, which is dependent on g^{n_1} and therefore relies on n_1, and a function $\widehat{f} \in \mathcal{F}^{n_2^*}$, such that

$$\|\frac{u - g^{n_1}}{\ell} - \widehat{f}\|_{1,p,\Omega} < \frac{\varepsilon^2}{\|\ell\|_{1,p,\Omega}}. \tag{26}$$

Correspondingly, the function $\widehat{w} = g^{n_1} + \ell\widehat{f} \in \mathcal{H}^{n_1,n_2^*}$ satisfies

$$\|u - \widehat{w}\|_{1,p,\Omega} = \|\ell(\frac{u - g^{n_1}}{\ell} - \widehat{f})\|_{1,p,\Omega} \leq \|\ell\|_{1,p,\Omega}\|\frac{u - g^{n_1}}{\ell} - \widehat{f}\|_{1,p,\Omega} < \varepsilon^2. \tag{27}$$

It then follows that

$$\inf_{w\in\mathcal{H}^{n_1,n_2}} \|u - w\|_{1,p,\Omega}^{1/2} \leq \|u - \widehat{w}\|_{1,p,\Omega}^{1/2} < \varepsilon, \quad \forall n_2 \geq n_2^*(n_1). \tag{28}$$

Finally, we make use of reduction to absurdity to prove that $\|u - u^{n_1,n_2}\|_{1,p,\Omega}$ can be arbitrarily small so long as n_1 and n_2 are large enough. Suppose that for all $n_1 > 0$ and $n_2 > 0$, there exists a constant $\delta > 0$, such that $\|u - u^{n_1,n_2}\|_{1,p,\Omega} \geq \delta$. If $\delta \leq 1$, according to (25) and (28), there exist integers $\widehat{n}_1 > 0$ and $\widehat{n}_2 > 0$ ($\widehat{n}_2$ is dependent on $\widehat{n}_1$), such that $\|u - u^{\widehat{n}_1,\widehat{n}_2}\|_{0,2,\Gamma_D} < \dfrac{\delta}{2C_5}$ and $\inf\limits_{w\in\mathcal{H}^{\widehat{n}_1,\widehat{n}_2}} \|u - w\|_{1,p,\Omega}^{1/2} < \dfrac{\delta^{(5-p)/4}}{2C_5}$. Then we have

$$\begin{aligned}
&\left(\frac{\|u - u^{\widehat{n}_1,\widehat{n}_2}\|_{1,p,\Omega}}{C_5} - \|u - u^{\widehat{n}_1,\widehat{n}_2}\|_{0,2,\Gamma_D}\right) \Big/ \inf_{w\in\mathcal{H}^{\widehat{n}_1,\widehat{n}_2}} \|u - w\|_{1,p,\Omega}^{1/2} > \delta^{(p-1)/4} \geq \delta^{(p-1)/2} \\
\Leftrightarrow\ & \|u - u^{\widehat{n}_1,\widehat{n}_2}\|_{1,p,\Omega} > C_5\left(\|u - u^{\widehat{n}_1,\widehat{n}_2}\|_{1,p,\Omega}^{(p-1)/2} \inf_{w\in\mathcal{H}^{\widehat{n}_1,\widehat{n}_2}} \|u - w\|_{1,p,\Omega}^{1/2} + \|u - u^{\widehat{n}_1,\widehat{n}_2}\|_{0,2,\Gamma_D}\right),
\end{aligned} \tag{29}$$

which is contradictory to (24). Hence, δ is not a lower bound of $\|u - u^{\widehat{n}_1,\widehat{n}_2}\|_{1,p,\Omega}$. Similarly, if $\delta > 1$, there exist an integer $\widehat{n}_1 > 0$ and a corresponding $\widehat{n}_2 > 0$, such that $\|u - u^{\widehat{n}_1,\widehat{n}_2}\|_{0,2,\Gamma_D} < \dfrac{\delta}{2C_5}$, $\inf\limits_{w\in\mathcal{H}^{\widehat{n}_1,\widehat{n}_2}} \|u - w\|_{1,p,\Omega}^{1/2} < \dfrac{\delta^{1/2}}{2C_5}$ and

$$\begin{aligned}
&\left(\frac{\|u - u^{\widehat{n}_1,\widehat{n}_2}\|_{1,p,\Omega}}{C_5} - \|u - u^{\widehat{n}_1,\widehat{n}_2}\|_{0,2,\Gamma_D}\right) \Big/ \inf_{w\in\mathcal{H}^{\widehat{n}_1,\widehat{n}_2}} \|u - w\|_{1,p,\Omega}^{1/2} > \delta^{1/2} > \delta^{(p-1)/2} \\
\Leftrightarrow\ & \|u - u^{\widehat{n}_1,\widehat{n}_2}\|_{1,p,\Omega} > C_5\left(\|u - u^{\widehat{n}_1,\widehat{n}_2}\|_{1,p,\Omega}^{(p-1)/2} \inf_{w\in\mathcal{H}^{\widehat{n}_1,\widehat{n}_2}} \|u - w\|_{1,p,\Omega}^{1/2} + \|u - u^{\widehat{n}_1,\widehat{n}_2}\|_{0,2,\Gamma_D}\right),
\end{aligned} \tag{30}$$

which is also in contradiction with (24). Therefore we can conclude that $\|u - u^{n_1,n_2}\|_{1,p,\Omega} \to 0$ as $n_1 \to \infty$ and $n_2 \to \infty$. □

We remark there that although only neural networks with single hidden layers are considered here, similar conclusions can be made for the case of multi-layer neural networks. The details are omitted for brevity. It is also worth noting that the assumptions in the analysis are only sufficient conditions for the converge of the PFNN method. Later numerical experiments with cases that the assumptions are not fully satisfied will show that the proposed PFNN method still works well.

4. Comparison with other methods

Most of the existing neural network methodologies employ a penalty method to deal with the essential boundary conditions. For the boundary-value problem (1), a straightforward way is to minimize the following energy functional in least-squares form:

$$\begin{aligned} I[w] \;:=& \int_\Omega \Big(-\nabla\cdot(\rho(|\nabla w|)\nabla w) + h(w)\Big)^2 d\boldsymbol{x} + \beta_1 \int_{\Gamma_D} (\varphi - w)^2 d\boldsymbol{x} \\ &+ \beta_2 \int_{\Gamma_N} \Big((\rho(|\nabla w|)\nabla w)\cdot \boldsymbol{n} - \psi\Big)^2 d\boldsymbol{x}, \end{aligned} \tag{31}$$

where β_1 and β_2 are penalty coefficients, which can also be seen as Lagrangian multipliers that help transform a constrained optimization problem into an unconstrained one.

Such least-squares approach has not only been adopted in many early studies [23, 24, 26, 28, 29, 32], but also employed by a number of recent works based on deep neural networks. An example is the physics-informed neural networks [40] in which deep neural networks are applied to solve forward and inverse problems involving nonlinear partial differential equations arising from thermodynamic, fluid mechanics and quantum mechanics. Following it, in the work of the hidden fluid mechanics [39] impressive results are obtained by extracting velocity and pressure information from the data of flow visualizations. Another example of using least-squares energy functionals is the work of the Deep Galerkin method [41], in which efforts are made to merge deep learning techniques with the Galerkin method for efficiently solving several high-dimensional differential equations. Overall, a major difficulty by using the least-squares approach is that approximations have to be made to the high-order derivatives of the true solution in some way, which could eventually lead to high training cost and low accuracy.

To avoid approximating high-order derivatives, several methods have been proposed to transform the original problem into the corresponding weak forms. Examples include the Deep Ritz method [36] which employs an energy functional of the Ritz type:

$$I[w] := \int_\Omega \left(P(w) + H(w)\right) d\boldsymbol{x} - \int_{\Gamma_N} \psi w d\boldsymbol{x} + \beta \int_{\Gamma_D} (\varphi - w)^2 d\boldsymbol{x}, \tag{32}$$

and the Deep Nitsche method [37] which is based on an energy functional in the sense of Nitsche:

$$\begin{aligned} I[w] :=\; & \int_\Omega \left(P(w) + H(w)\right) d\boldsymbol{x} - \int_{\Gamma_N} \psi w d\boldsymbol{x} - \int_{\Gamma_D} w\Big(\rho(|\nabla w|)\nabla w\cdot \boldsymbol{n}\Big) d\boldsymbol{x} \\ & - \int_{\Gamma_D} \varphi\left(\beta w - \Big(\rho(|\nabla w|)\nabla w\cdot \boldsymbol{n}\Big)\right) d\boldsymbol{x} + \frac{\beta}{2}\int_{\Gamma_D} w^2 d\boldsymbol{x}. \end{aligned} \tag{33}$$

The transformations to weak forms done in the two methods can effectively reduce the smoothness requirement of the approximate solution. However, the penalty terms due to the essential boundary condition still persist, which would lead to extra training cost. Moreover, there is little clue on how to set the penalty factor β; improper values will cause negative influence on the accuracy of the approximate solution or even lead to training failure.

There are also several attempts [24, 25, 26, 27] made to eliminate the penalty terms by explicitly manufacturing an approximate solution in the following form:

$$w_{\boldsymbol{\theta}}(\boldsymbol{x}) = \mathcal{G}(\boldsymbol{x}) + \mathcal{L}(\boldsymbol{x}) f_{\boldsymbol{\theta}}(\boldsymbol{x}), \tag{34}$$

where $\mathcal{G}$ satisfies the essential boundary condition and $\mathcal{L}$ serves as a length factor function. It is worth noting that the scopes of applications of these methods are rather narrow, despite that the approximate solutions do share some similarities with the PFNN method. In particular, these methods usually construct function $\mathcal{G}$ either in analytic forms [24, 25], or through spline interpolations [26, 27], and are therefore only suitable to simple geometries in low dimensions. To establish the length factor function $\mathcal{L}$, these methods usually rely on mapping the original domain to a hyper-sphere, which is again not flexible and efficient for problems with complex geometries and high dimensions.

The proposed PFNN method can effectively combine the advantages of the aforementioned state-of-the-art while overcoming their drawbacks. It reduces the smoothness requirements as well as removes the penalty term in the loss function, effectively converting the original hard problem to a relatively easy one. By introducing two neural networks, instead of only one, the approximations made to the true solutions are separated to the essential boundaries and the rest of the domain, respectively. The original training task is divided into two simpler ones, which can substantially reduce the training cost as well as enhance the accuracy of the approximation. To eliminate the interference between the two neural networks, a systematic approach is further proposed to construct the length factor function in a most flexible manner. As we will show later in the numerical experiments, the PFNN method is applicable to a wide range of problems on complex geometries in arbitrary dimensions and is able to achieve higher accuracy with lower training cost as compared with other approaches.

5. Numerical experiments

Table 1: List of test cases for numerical experiments.

Case	Problem	Dimension	Domain	$\rho(\lvert\nabla u\rvert)$	$h(u)$
1	anisotropic diffusion	2	square	$\boldsymbol{A}$	c
2	minimal surface	2	Koch snowflake	$1/\sqrt{1+\lvert\nabla u\rvert^2}$	0
3	p-Liouville-Bratu	3	twisted torus	$\lvert\nabla u\rvert^{p-2}$	$-\lambda\exp(u)+c$
4	p-Helmholtz	100	hypercube	$\lvert\nabla u\rvert^{p-2}$	$u+c$

A series of numerical experiments are conducted to examine the numerical behaviors of the proposed PFNN method as well as several previous state-of-the-art approaches. We design four test cases covering different types of problems that have the same form of (1) but vary in $\rho(|\nabla u|)$ and $h(u)$, as shown in Table 1. In particular, the computational domains of test cases 2 and 3 are further illustrated in Figure 2, both exhibiting very complex geometries. We employ the ResNet model [51] with sinusoid activation functions to build the neural

networks in both PFNN and other neural network based methods. The Adam optimizer [52] is utilized for training, with the initial learning rate set to 0.01. Unless mentioned otherwise, the maximum number of iteration is set to 5,000 epochs. The relative ℓ_2-norm is used to estimate the error of the approximate solution. In all tests except those with the traditional finite element method, we perform ten independent tests and collect the results for further analysis.

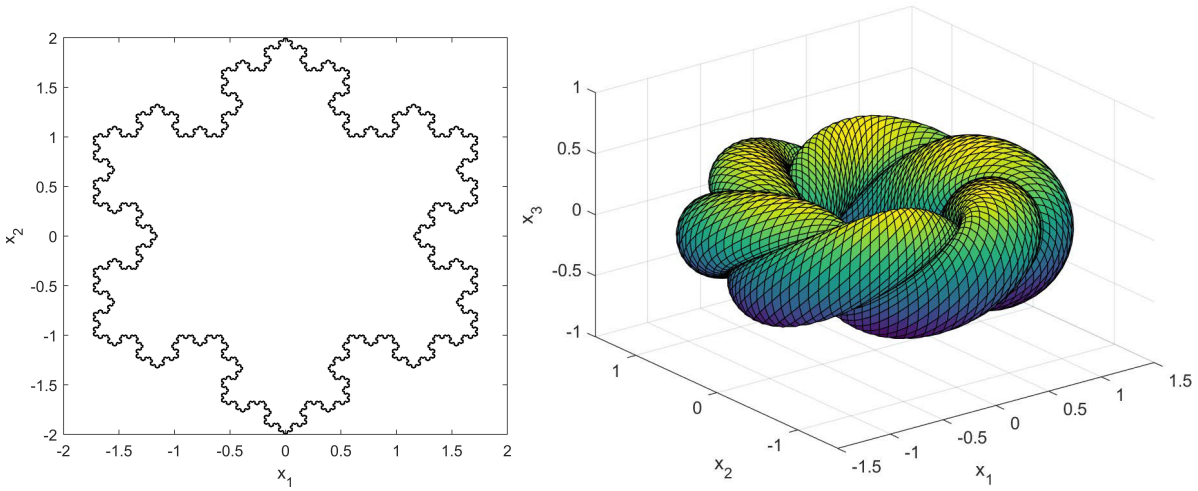

(a) Koch snowflake ($L = 5$) (b) Twisted torus

Figure 2: The computation domains with complex geometries in test cases 2 (a) and 3 (b).

5.1. Anisotropic diffusion equation on a square

The first test case is an anisotropic diffusion equation:

$$-\nabla \cdot \boldsymbol{A}\nabla u + c = 0 \quad \text{in } \Omega = [-1, 1]^2, \tag{35}$$

where

$$\boldsymbol{A} = \begin{bmatrix} (x_1 + x_2)^2 + 1 & -(x_1^2 + x_2^2) \\ -(x_1^2 + x_2^2) & (x_1 - x_2)^2 + 1 \end{bmatrix}. \tag{36}$$

The corresponding energy functional to minimize is:

$$\Psi[w] = \int_\Omega (\boldsymbol{A}\nabla w \cdot \nabla w + cw) d\boldsymbol{x} - \int_{\Gamma_N} \psi w d\boldsymbol{x}. \tag{37}$$

In the experiment, we set the essential boundary to $\Gamma_D = \{-1\} \times [-1, 1]$ and set the exact solution to various forms including $u^{(1)} = \ln(10(x_1 + x_2)^2 + (x_1 - x_2)^2 + 0.5)$, $u^{(2)} = (x_1^3 - x_1)\cosh(2x_2)$, $u^{(3)} = (x_1^2 - x_2^2)/(x_1^2 + x_2^2 + 0.1)$, and $u^{(4)} = (\operatorname{sign} x_1)\left((x_1 + \operatorname{sign} x_1)^4 - 1\right)\exp(-x_2^2)$, where $u^{(4)}$, discontinuous as such, is a weak solution of the partial differential equation.

For comparison purpose, we examine the performance of several approaches including the linear finite element method, the least-squares neural network method, the Deep Ritz

method, the Deep Nitsche method and our proposed PFNN method. A uniform mesh of 30×30 cells is used by the bilinear finite element method, leading to $31\times30=930$ unknowns. For the penalty-based neural network methods, the network adopted is comprised of 4 ResNet blocks, each of which contains 2 fully connected layers with 10 units and a residual connection, resulted in totally 811 undecided parameters. And for the PFNN method, the network $g_{\boldsymbol{\theta_1}}$ and $f_{\boldsymbol{\theta_2}}$ consist of 1 and 3 ResNet blocks, respectively, corresponding to a total of $151+591=742$ parameters. The penalty coefficients in the penalty-based approaches are all set to three typical values: 100, 300 and 500.

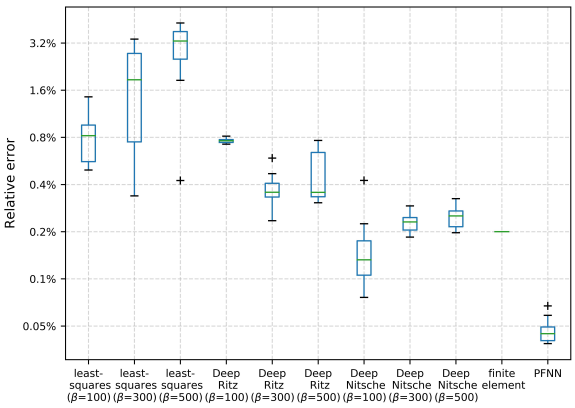

(a) $u^{(1)}=\ln(10(x_1+x_2)^2+(x_1-x_2)^2+0.5)$

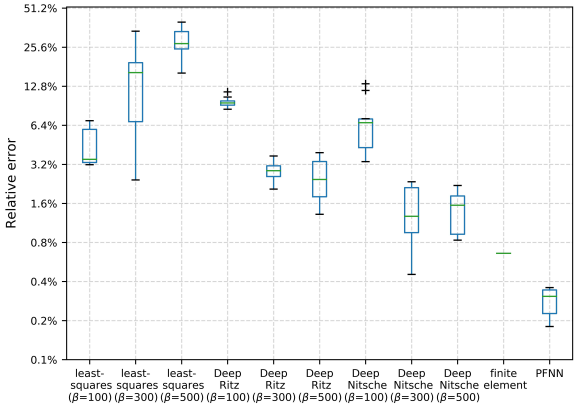

(b) $u^{(2)}=(x_1^3-x_1)\cosh(2x_2)$

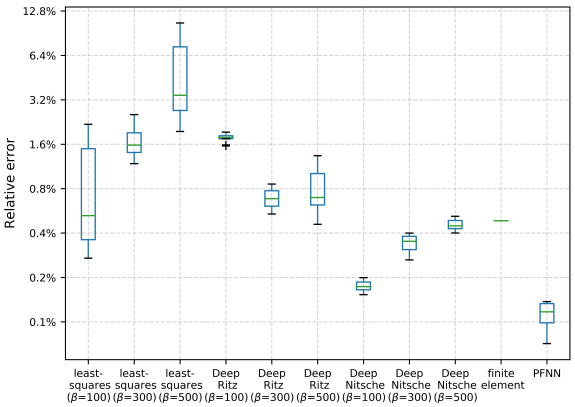

(c) $u^{(3)}=(x_1^2-x_2^2)/(x_1^2+x_2^2+0.1)$

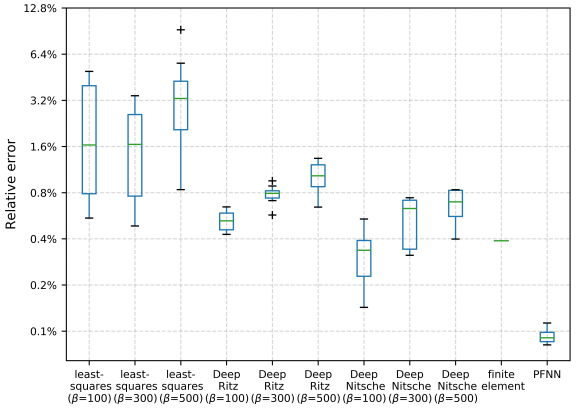

(d) $u^{(4)}=\mathrm{sign}(x_1)\Big((x_1+\mathrm{sign}(x_1))^4-1\Big)\exp(-x_2^2)$

Figure 3: Results of solving the anisotropic diffusion equation on a square with various methods.

The experiment results are illustrated in Figure 3. To get detailed information of the achievable accuracy of every approach, we draw in the figure the box-plots that contain the five-number summary including the smallest observation, lower quartile, median, upper quartile, and largest observation for each set of tests. From the figure, it can be observed that

the performance of the classical least-squares neural network method is usually the worst, due in large part to the approximations made to high-oder derivatives. By introducing the corresponding weak forms, Deep Ritz and Deep Nitsche methods can deliver better results than the least-squares method does, but the performance still has a strong dependency on the specific values of the penalty coefficients and the performance is in many cases not competitive to the traditional finite element method. The advantages of the PFNN method are quite clear: it is able to outperform all above approaches in all tested problems in terms of the sustained accuracy and is much more robust than the penalty-based methods.

5.2. Minimal surface equation on a Koch snowflake

Consider a minimal surface equation [53]:

$$-\nabla\cdot\left(\frac{\nabla u}{\sqrt{1+|\nabla u|^2}}\right)=0, \tag{38}$$

defined on a well-known fractal pattern – the Koch snowflake domain [54], as shown in Figure 2 (a). The equation (38) can be seen as the Euler-Lagrange equation of the energy functional:

$$\Psi[w]:=\int_\Omega\sqrt{1+|\nabla w|^2}dx, \tag{39}$$

which represents the area of the surface of w on Ω.

The minimal surface problem is to find a surface with minimal area under the given boundary conditions. It can be verified that the catenoid surface

$$u=\lambda\cosh(\frac{x_1}{\lambda})\sqrt{1-z^2},\quad z=\left(\frac{x_2}{\lambda\cosh(x_1/\lambda)}\right) \tag{40}$$

satisfies the equation (38) for all λ satisfying $|z|\leq 1$ in Ω. In particular, for the Koch snowflake, the condition becomes $\lambda\geq 2$. The difficulty of the problem is increased as $\lambda\to 2$ (especially, $|\nabla u|$ is unbounded on Ω when $\lambda=2$). To examine how well various methods can deal with such kind of problem, we set λ to a relatively challenging value: $\lambda=2.1$.

In the experiment, we set the essential boundary Γ_D to be the left half part of the boundary and gradually increase the fractal level L of the Koch polygon. With L increased, the number of segments on the boundary of the domain grows exponentially [54], posing severe challenges to classical approaches such as the finite element method. Thanks to the meshfree nature, neural network methods could be more suitable to tackle this problem. We investigate the performance of the Deep Ritz, Deep Nitsche and PFNN methods with $L=5$, 6 and 7. The configurations of the neural networks are the same to those in the previous experiment. We report both mean values and standard deviations of the solution errors of all the approaches in Table 2, from which we can see that PFNN can achieve the most accurate results with the least number of parameters and is much less susceptible to the change of domain boundary.

Table 2: Errors of various methods for solving the minimal surface equation on a Koch snowflake.

Method	Deep Ritz		Deep Nitsche		PFNN
Unknowns	811		811		742
$L=5$	$\beta=100$	0.454%±0.072%	$\beta=100$	0.535%±0.052%	**0.288%±0.030%**
	$\beta=300$	1.763%±0.675%	$\beta=300$	1.164%±0.228%	
	$\beta=500$	5.245%±1.943%	$\beta=500$	3.092%±1.256%	
$L=6$	$\beta=100$	0.747%±0.101%	$\beta=100$	0.483%±0.095%	**0.309%±0.064%**
	$\beta=300$	3.368%±0.690%	$\beta=300$	0.784%±0.167%	
	$\beta=500$	4.027%±1.346%	$\beta=500$	2.387%±0.480%	
$L=7$	$\beta=100$	0.788%±0.041%	$\beta=100$	0.667%±0.149%	**0.313%±0.071%**
	$\beta=300$	2.716%±0.489%	$\beta=300$	1.527%±0.435%	
	$\beta=500$	4.652%±1.624%	$\beta=500$	1.875%±0.653%	

5.3. p-Liouville-Bratu equation on a twisted torus

The next test case is a Dirichlet boundary-value problem governed by a p-Liouville-Bratu equation:

$$-\nabla\cdot\left(|\nabla u|^{p-2}\nabla u\right)-\lambda\exp(u)+c=0, \tag{41}$$

where $p>1$ and $\lambda\geq 0$. This equation can be transformed to a minimization problem of the following energy functional:

$$\Psi[w]:=\int_{\Omega}\left(\frac{1}{p}|\nabla w|^{p}-\lambda\exp(w)+cw\right)dx. \tag{42}$$

The computational domain is a twisted torus as shown in Figure 2 (b), for which the parameter equation of the boundary is:

$$\begin{cases} x_1=(r_0+s_1\cos(\vartheta_1)-s_2\sin(\vartheta_1))\cos(\vartheta_1/3),\\ x_2=(r_0+s_1\cos(\vartheta_1)-s_2\sin(\vartheta_1))\sin(\vartheta_1/3),\\ x_3=s_1\sin(\vartheta_1)+s_2\cos(\vartheta_1), \end{cases} \tag{43}$$

where

$$\begin{cases} s_1=(r_1+r_2)\cos(\vartheta_2)-r_2\cos\left(\dfrac{r_1+r_2}{r_2}\vartheta_2\right),\\ s_2=(r_1+r_2)\sin(\vartheta_2)-r_2\sin\left(\dfrac{r_1+r_2}{r_2}\vartheta_2\right), \end{cases} \tag{44}$$

$\vartheta_1\in[0,6\pi]$, $\vartheta_2\in[0,2\pi]$, $r_0=1$, $r_1=1/4$ and $r_2=1/8$.

When $p=2$, the p-Liouville-Bratu equation is degenerated to the well-known Liouville-Bratu equation [55]. The nonlinearity of the problem is increased as p deviates from 2. In particular, if $1<p<2$, the diffusivity $|\nabla u|^{p-2}\to\infty$ as $|\nabla u|\to 0$. And if $p>2$ (especially for $p>3$), the diffusivity $|\nabla u|^{p-2}$ grows dramatically as $|\nabla u|$ increases. In both cases, the corresponding p-Liouville-Bratu equation is difficult to solve, let alone that the computational domain is also very complex. In addition, the nonlinearity of the problem is

also raised as the Bratu parameter λ becomes larger. One thing worth noting is that here $h(u) = -\lambda \exp(u) + c$ is a decreasing function. Arbitrarily large λ could make the solution of (41) not be the minimal point of the energy functional (42). However, if λ is restricted in a proper range, it is still feasible to obtain a solution by minimizing the equivalent optimization problem.

In the experiment, we set the exact solution to be $u = ((x_1^3 - 3x_1)(x_2^3 - 3x_2) - 3)(x_3^3 + 3)$ and conduct two groups of tests to investigate the performance of various neural network methods in solving the p-Liouville-Bratu equation (41) with parameter $p = 1.5$ and $p = 4.0$, respectively. In each group of tests, we examine the influence of the Bratu parameter with $\lambda = 0.6$ and $\lambda = 1.2$, respectively. Again, the configurations of the neural networks are the same to those in the previous experiment. The test results are reported in Table 3. From the table, we can clearly see that the proposed PFNN method can outperform the other two methods with less parameters used. In particular, for the case of $p = 4.0$, both Deep Ritz and Deep Nitsche suffer greatly from the high nonlinearity of the problem and could not produce accurate results, while PFNN can perform equally well with the change of both p and λ.

Table 3: Errors of various methods for solving the p-Liouville-Bratu equation on a twisted torus.

Method		Deep Ritz		Deep Nitsche		PFNN
Unknowns		821		821		762
$p = 1.5$	$\lambda = 0.6$	$\beta = 100$	0.653%±0.028%	$\beta = 100$	0.707%±0.058%	**0.463%±0.038%**
		$\beta = 300$	0.688%±0.051%	$\beta = 300$	0.685%±0.047%	
		$\beta = 500$	0.713%±0.073%	$\beta = 500$	0.728%±0.018%	
	$\lambda = 1.2$	$\beta = 100$	0.681%±0.022%	$\beta = 100$	0.717%±0.031%	**0.472%±0.044%**
		$\beta = 300$	0.679%±0.034%	$\beta = 300$	0.706%±0.039%	
		$\beta = 500$	0.694%±0.029%	$\beta = 500$	0.698%±0.044%	
$p = 4.0$	$\lambda = 0.6$	$\beta = 100$	5.964%±0.045%	$\beta = 100$	7.094%±0.183%	**0.372%±0.055%**
		$\beta = 300$	3.825%±0.032%	$\beta = 300$	5.639%±0.174%	
		$\beta = 500$	2.869%±0.047%	$\beta = 500$	3.872%±0.284%	
	$\lambda = 1.2$	$\beta = 100$	6.234%±0.065%	$\beta = 100$	7.125%±0.196%	**0.361%±0.047%**
		$\beta = 300$	3.976%±0.059%	$\beta = 300$	5.356%±0.218%	
		$\beta = 500$	3.114%±0.052%	$\beta = 500$	4.233%±0.237%	

5.4. p-Helmhotz equation on a 100D hypercube

In the last experiment, consider a mixed boundary-value problem governed by a p-Helmholtz equation ($p > 1$, $\alpha = 2$):

$$\begin{cases} -\nabla \cdot \left(|\nabla u|^{p-2} \nabla u \right) + u + c = 0, & \text{in } \Omega, \\ u = \varphi, & \text{on } \Gamma_D, \\ \left(|\nabla u|^{p-2} \nabla u \right) \cdot \boldsymbol{n} + \alpha u = \psi, & \text{on } \Gamma_R, \end{cases} \tag{45}$$

where Ω is a 100D hypercube $[0,1]^{100}$ and Γ_R represents the Robin boundary. For this problem, the corresponding energy functional to minimize is:

$$\Psi[w] := \int_\Omega \left(\frac{1}{p}|\nabla w|^p + \frac{1}{2}w^2 + cw \right) dx + \int_{\Gamma_R} \left(\frac{1}{2}\alpha w^2 - \psi w \right) dx. \tag{46}$$

In the experiment we set the exact solution to

$$u = \frac{1}{100} \left(\sum_{j=1}^{99} \exp\left(-(x_j^2 + x_{j+1}^2)\right) + \exp\left(-(x_{100}^2 + x_1^2)\right) \right)$$

and the Dirichlet boundary to be $\Gamma_D = \cup_{j=1}^{100} \{\boldsymbol{x} | x_j = 0\}$. Three groups of tests are carried out, with parameter $p = 1.2$, 3.6 and 4.8, respectively. For $p = 1.2$ and $p = 3.6$, the maximum number of iterations is set to 20,000 epochs, while for the case that $p = 4.8$, it is increased to $40,000$ epochs since the problem becomes more difficult. At each step of the iteration, $5,000$ points in the domain and 50 points on each hyper-plane that belongs to the boundary are sampled to form the training set.

We apply the Deep Ritz, Deep Nitsche and PFNN methods and compare their performance on this high-dimensional problem. The network structures for the Deep Ritz and Deep Nitsche methods are the same, both consisting of 4 ResNet blocks of width 120, resulting in $113,881$ undecided parameters. And the PFNN method employs two neural networks that are comprised of 1 and 3 blocks of width 120, respectively, corresponding to a total of $26,761 + 84,841 = 111,602$ unknowns. The penalty factors in Deep Ritz and Deep Nitsche are set to three typical values: $\beta = 1000$, 3000 and 5000. The relative errors of the tree tested approaches are listed in Table 4, which again demonstrate the advantages of the proposed PFNN method in terms of both accuracy and robustness. To further examine the efficiency of various methods, we draw the evolution history of the relative errors in Figure 4. The figure clearly indicates that PFNN is not only more accurate, but also has a faster convergence speed across all tests.

Table 4: Errors of various methods for solving the p-Helmholtz equation on a 100D hypercube.

Method	Deep Ritz		Deep Nitsche		PFNN
Unknowns	113,881		113,881		111,602
$p = 1.2$	$\beta = 1,000$	1.405%±0.091%	$\beta = 1,000$	1.424%±0.078%	**1.026%±0.083%**
	$\beta = 3,000$	1.529%±0.088%	$\beta = 3,000$	1.498%±0.082%	
	$\beta = 5,000$	1.655%±0.084%	$\beta = 5,000$	1.487%±0.086%	
$p = 3.6$	$\beta = 1,000$	5.192%±0.062%	$\beta = 1,000$	5.199%±0.071%	**1.037%±0.072%**
	$\beta = 3,000$	5.266%±0.055%	$\beta = 3,000$	5.133%±0.063%	
	$\beta = 5,000$	5.203%±0.058%	$\beta = 5,000$	5.165%±0.069%	
$p = 4.8$	$\beta = 1,000$	5.206%±0.049%	$\beta = 1,000$	5.263%±0.057%	**0.780%±0.067%**
	$\beta = 3,000$	5.180%±0.061%	$\beta = 3,000$	5.169%±0.044%	
	$\beta = 5,000$	5.214%±0.053%	$\beta = 5,000$	5.187%±0.055%	

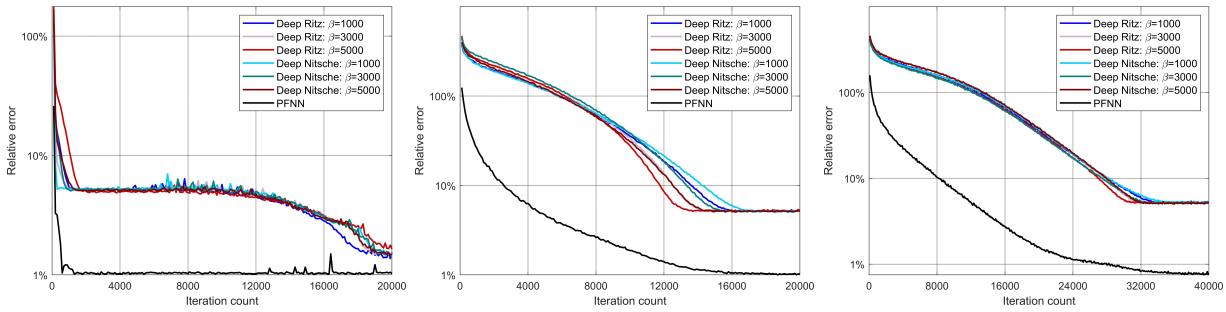

(a) $p = 1.2$ (b) $p = 3.6$ (c) $p = 4.8$

Figure 4: Error evolution history of various methods during the training process.

6. Conclusion

In this paper, we proposed PFNN – a penalty-free neural network method to solve a class of second-order boundary-value problems on complex geometries. By using the PFNN method the original problem is transformed to a weak form without any penalty terms and the solution is constructed with two networks and a length factor function. We provide a theoretical analysis to prove that PFNN is convergent as the number of hidden units of the networks increases and present a series of numerical experiments to demonstrate that the PFNN method is not only more accurate and flexible, but also more robust than the previous state-of-the-art. Possible future works on PFNN could include further theoretical analysis of the convergence speed and stability, further improvement on the training technique and further study on the corresponding parallel algorithm for solving larger problems on high-performance computers.

Acknowledgements

This study was funded in part by Beijing Natural Science Foundation (#JQ18001), Guangdong Key R&D Project (#2019B121204008) and Beijing Academy of Artificial Intelligence.

References

[1] I. Goodfellow, Y. Bengio, A. Courville, Deep learning, MIT Press, 2016.
[2] Y. LeCun, Y. Bengio, G. Hinton, Deep learning, Nature 521 (2015) 436–444.
[3] J. Schmidhuber, Deep learning in neural networks: An overview, Neural Networks 61 (2015) 85–117.
[4] M. I. Razzak, S. Naz, A. Zaib, Deep learning for medical image processing: Overview, challenges and the future, in: Classification in BioApps, Springer, 2018, pp. 323–350.
[5] A. Voulodimos, N. Doulamis, A. Doulamis, E. Protopapadakis, Deep learning for computer vision: A brief review, Computational Intelligence and Neuroscience 2018 (2018).
[6] T. Young, D. Hazarika, S. Poria, E. Cambria, Recent trends in deep learning based natural language processing, IEEE Computational Intelligence Magazine 13 (2018) 55–75.
[7] J. Ling, A. Kurzawski, J. Templeton, Reynolds averaged turbulence modelling using deep neural networks with embedded invariance, Journal of Fluid Mechanics 807 (2016) 155–166.

[8] K. Duraisamy, G. Iaccarino, H. Xiao, Turbulence modeling in the age of data, Annual Review of Fluid Mechanics 51 (2019) 357–377.
[9] L. Zhang, J. Han, H. Wang, R. Car, W. E, Deep potential molecular dynamics: A scalable model with the accuracy of quantum mechanics, Physical Review Letters 120 (2018) 143001.
[10] L. Li, J. C. Snyder, I. M. Pelaschier, J. Huang, U.-N. Niranjan, P. Duncan, M. Rupp, K.-R. Müller, K. Burke, Understanding machine-learned density functionals, International Journal of Quantum Chemistry 116 (2016) 819–833.
[11] W. E, J. Han, A. Jentzen, Deep learning-based numerical methods for high-dimensional parabolic partial differential equations and backward stochastic differential equations, Communications in Mathematics and Statistics 5 (2017) 349–380.
[12] J. Han, A. Jentzen, W. E, Solving high-dimensional partial differential equations using deep learning, Proceedings of the National Academy of Sciences 115 (2018) 8505–8510.
[13] M. Raissi, Forward-backward stochastic neural networks: Deep learning of high-dimensional partial differential equations, arXiv preprint arXiv:1804.07010 (2018).
[14] C. Beck, W. E, A. Jentzen, Machine learning approximation algorithms for high-dimensional fully nonlinear partial differential equations and second-order backward stochastic differential equations, Journal of Nonlinear Science 29 (2019) 1563–1619.
[15] J. He, L. Li, J. Xu, C. Zheng, ReLU deep neural networks and linear finite elements, Journal of Computational Mathematics (2019).
[16] Y. Fan, C. O. Bohorquez, L. Ying, Bcr-net: A neural network based on the nonstandard wavelet form, Journal of Computational Physics 384 (2019) 1–15.
[17] J. He, J. Xu, Mgnet: A unified framework of multigrid and convolutional neural network, Science China Mathematics 62 (2019) 1331–1354.
[18] Y. Fan, L. Lin, L. Ying, L. Zepeda-Núnez, A multiscale neural network based on hierarchical matrices, Multiscale Modeling & Simulation 17 (2019) 1189–1213.
[19] Y. Fan, J. Feliu-Faba, L. Lin, L. Ying, L. Zepeda-Núnez, A multiscale neural network based on hierarchical nested bases, Research in the Mathematical Sciences 6 (2019) 21.
[20] K. Li, K. Tang, T. Wu, Q. Liao, D3M: A deep domain decomposition method for partial differential equations, IEEE Access (2019).
[21] H. Lee, I. S. Kang, Neural algorithm for solving differential equations, Journal of Computational Physics 91 (1990) 110–131.
[22] A. J. Meade Jr, A. A. Fernandez, The numerical solution of linear ordinary differential equations by feedforward neural networks, Mathematical and Computer Modelling 19 (1994) 1–25.
[23] B. P. van Milligen, V. Tribaldos, J. Jiménez, Neural network differential equation and plasma equilibrium solver, Physical Review Letters 75 (1995) 3594.
[24] I. E. Lagaris, A. Likas, D. I. Fotiadis, Artificial neural networks for solving ordinary and partial differential equations, IEEE Transactions on Neural Networks 9 (1998) 987–1000.
[25] I. E. Lagaris, A. C. Likas, D. G. Papageorgiou, Neural-network methods for boundary value problems with irregular boundaries, IEEE Transactions on Neural Networks 11 (2000) 1041–1049.
[26] K. S. McFall, J. R. Mahan, Artificial neural network method for solution of boundary value problems with exact satisfaction of arbitrary boundary conditions, IEEE Transactions on Neural Networks 20 (2009) 1221–1233.
[27] K. S. McFall, Automated design parameter selection for neural networks solving coupled partial differential equations with discontinuities, Journal of the Franklin Institute 350 (2013) 300–317.
[28] L. Jianyu, L. Siwei, Q. Yingjian, H. Yaping, Numerical solution of differential equations by radial basis function neural networks, in: Proceedings of the 2002 International Joint Conference on Neural Networks. IJCNN'02 (Cat. No. 02CH37290), volume 1, IEEE, 2002, pp. 773–777.
[29] N. Mai-Duy, T. Tran-Cong, Numerical solution of differential equations using multiquadric radial basis function networks, Neural Networks 14 (2001) 185–199.
[30] P. Ramuhalli, L. Udpa, S. S. Udpa, Finite-element neural networks for solving differential equations, IEEE Transactions on Neural Networks 16 (2005) 1381–1392.

[31] L. O. Chua, L. Yang, Cellular neural networks: Theory, IEEE Transactions on Circuits and Systems 35 (1988) 1257–1272.
[32] X. Li, J. Ouyang, Q. Li, J. Ren, Integration wavelet neural network for steady convection dominated diffusion problem, in: 2010 Third International Conference on Information and Computing, volume 2, IEEE, 2010, pp. 109–112.
[33] M. A. Nielsen, Neural networks and deep learning, volume 2018, Determination press San Francisco, CA, USA:, 2015.
[34] C. C. Aggarwal, Neural networks and deep learning, Springer 10 (2018) 978–3.
[35] C. F. Higham, D. J. Higham, Deep learning: An introduction for applied mathematicians, SIAM Review 61 (2019) 860–891.
[36] W. E, B. Yu, The Deep Ritz method: A deep learning-based numerical algorithm for solving variational problems, Communications in Mathematics and Statistics 6 (2018) 1–12.
[37] Y. Liao, P. Ming, Deep Nitsche method: Deep Ritz method with essential boundary conditions, arXiv preprint arXiv:1912.01309 (2019).
[38] Y. Zang, G. Bao, X. Ye, H. Zhou, Weak adversarial networks for high-dimensional partial differential equations, Journal of Computational Physics (2020) 109409.
[39] M. Raissi, A. Yazdani, G. E. Karniadakis, Hidden fluid mechanics: Learning velocity and pressure fields from flow visualizations, Science 367 (2020) 1026–1030.
[40] M. Raissi, P. Perdikaris, G. E. Karniadakis, Physics-informed neural networks: A deep learning framework for solving forward and inverse problems involving nonlinear partial differential equations, Journal of Computational Physics 378 (2019) 686–707.
[41] J. Sirignano, K. Spiliopoulos, DGM: A deep learning algorithm for solving partial differential equations, Journal of Computational Physics 375 (2018) 1339–1364.
[42] J. Berg, K. Nyström, A unified deep artificial neural network approach to partial differential equations in complex geometries, Neurocomputing 317 (2018) 28–41.
[43] Z. Long, Y. Lu, B. Dong, PDE-Net 2.0: Learning PDEs from data with a numeric-symbolic hybrid deep network, Journal of Computational Physics 399 (2019) 108925.
[44] J. N. Kani, A. H. Elsheikh, DR-RNN: A deep residual recurrent neural network for model reduction, arXiv preprint arXiv:1709.00939 (2017).
[45] Y. Khoo, J. Lu, L. Ying, Solving parametric PDE problems with artificial neural networks, arXiv preprint arXiv:1707.03351 (2017).
[46] G. B. Wright, Radial basis function interpolation: numerical and analytical developments, University of Colorado at Boulder, 2003.
[47] R. Franke, Scattered data interpolation: tests of some methods, Mathematics of Computation 38 (1982) 181–200.
[48] T. A. Foley, Interpolation and approximation of 3-D and 4-D scattered data, Computers & Mathematics with Applications 13 (1987) 711–740.
[49] S.-S. Chow, Finite element error estimates for non-linear elliptic equations of monotone type, Numerische Mathematik 54 (1989) 373–393.
[50] K. Hornik, Approximation capabilities of multilayer feedforward networks, Neural Networks 4 (1991) 251–257.
[51] K. He, X. Zhang, S. Ren, J. Sun, Deep residual learning for image recognition, in: Proceedings of the IEEE conference on computer vision and pattern recognition, 2016, pp. 770–778.
[52] D. P. Kingma, J. Ba, Adam: A method for stochastic optimization, arXiv preprint arXiv:1412.6980 (2014).
[53] E. Giusti, G. H. Williams, Minimal surfaces and functions of bounded variation, volume 80, Springer, 1984.
[54] H. Koch, Sur une courbe continue sans tangente, obtenue par une construction géométrique élémentaire, Arkiv for Matematik, Astronomi och Fysik 1 (1904) 681–704.
[55] G. Bratu, Sur les équations intégrales non linéaires, Bulletin de la Société Mathématique de France 42 (1914) 113–142.